Femtosecond Heterodyne-Detected Four-Wave-Mixing Studies of Deterministic Protein Motions. 2. Protein Response

Gregory D. Goodno[†]

Department of Physics and Astronomy, University of Rochester, Rochester, New York 14627

Vladimir Astinov and R. J. Dwayne Miller*

Departments of Chemistry and Physics, 80 St. George Street, University of Toronto, Toronto, Ontario M5S 3H6 Canada

Received: October 6, 1999

The initial structural evolution of carboxymyoglobin (MbCO) following photodissociation of CO is studied using optically heterodyne-detected (OHD) transient grating (TG) spectroscopy. This method provides detailed dynamical information on the electronic and structural states of the heme protein following photoexcitation. The phase anisotropy of MbCO is found to develop on subpicosecond to picosecond time scales and is much greater than can be attributed to the symmetry of the heme dipole transition. Control studies of carboxyprotoheme and deoxymyoglobin were used to identify the components due to protein structural relaxation and thermal relaxation, respectively. A geometric decomposition of the MbCO grating signals into contributions relative to the molecular axes provides evidence that the protein effectively changes its shape within 500 fs following ligand dissociation. These anisotropic mass displacements are a signature of functionally important motions since they imply a certain degree of directionality or mode selective coupling to the response. The anisotropic relaxation and observed dynamics provide further evidence that the low-frequency collective modes of proteins play an important role in transducing reaction forces into functions.

I. Introduction

As a first step in understanding the mechanics behind the spatial coupling of reaction coordinates inherent in molecular cooperativity,[1] it is important to understand the tertiary structural changes of individual proteins. With respect to the classic cooperative response of hemoglobin, myoglobin provides a model system for the tertiary relaxation processes. It is structurally very similar to the subunits of hemoglobin and is involved in oxygen transport in muscles. Equally important, it has nearly ideal optical properties for optically based dynamical studies. Notably, the excited-state surface of the ligated heme is dissociative such that it is possible to photoinitiate the oxy to deoxy structural relaxation within 50 fs with essentially unit quantum efficiency.[2] By the use of CO as the ligand rather than O_2, it is also possible to avoid geminate recombination processes from complicating the relaxation dynamics.[3] Thus, the carboxymyoglobin (MbCO) system is unique in that it gives access to the full range of protein relaxation processes to a single perturbation (ligand dissociation) without complicating side reactions and associated population dynamics. For this reason, an enormous body of work has accumulated on myoglobin relaxation processes that has helped establish general principles related to protein dynamics.

The following provides a brief summary of the most salient general features relevant to the present study. We know the protein's potential energy landscape is much more coarse grain than other highly associated systems such as glasses and can be described within a hierarchical model for the conformational distribution.[4] It is possible to identify classes of conformational substates that can be ordered in terms of relative importance with respect to particular observables. For example, there are distinct CO binding sites within the heme pocket at low temperature[4] that persist to room temperature.[5] The barrier distributions to geminate CO binding also show implications of modal behavior.[4] The most marked illustration of this effect has recently been observed in optical hole-burning studies of myoglobin where tiers in the temperature dependence are clearly observed in the line widths.[6] There are also "open" and "closed" conformational substate distributions with respect to the distal side of the Fe−ligand binding site[7] that may be important to ligand escape and entry into the protein. For systems as complex as proteins, there must be a broad distribution of conformations. The relatively new concept is that the distribution is strongly tiered with respect to the various observables. This hierarchical behavior is undoubtedly related to the distinctly different length scales of motion encoded in the protein structure. Glasses and other strongly associated homogeneous systems also have a broad range of length scales, but the activation barriers separating the different length scales is a continuous function of the length scale. In proteins, there is a significant difference in the degree of correlation and barrier distribution separating different length scales of motion for helical sections in comparison to loops in the structure. The correlations of atomic motions are much more pronounced in the helical regions than in the loop regions due to the additional attractive interactions imposed by the secondary structure. The barrier contours defining root mean square (rms) motions about the minimum in the vicinity of a helix are much steeper than in the loop regions. Since the number of helices or other secondary features in any protein structure is discrete, this effect leads naturally to a coarse grain distribution function. It is this strong variation

[†] Current address: TRW Space and Electronics Group, Redondo Beach, CA 90278.

10.1021/jp993559y CCC: $18.00
Published on Web 11/12/1999

in different length scales of motion and associated barrier distributions (i.e., structural heterogeneity) that is the greatest distinguishing feature between proteins and glasses. The question is how to map the conformational substate distribution onto the functional response of the protein. In a paradoxical fashion, the protein relaxation dynamics are found to exhibit stretched exponential behavior [$\exp[-(kt)^{\beta}]$] with stretch parameters (β) close to 0.6, which is characteristic of glasses.[7] The hierarchical behavior does not obviously manifest itself in the relaxation dynamics. Detailed studies of solvent viscosity have shown the protein motion to be "slaved" to the surrounding solvent.[8] The fluctuations must displace solvent and most likely involve changes in effective volume. Some of the glasslike behavior in the relaxation dynamics may reflect frictional interactions with the surrounding solvent. However, there is also evidence that the exact behavior depends on the probe transition used to follow the dynamics. Transitions sensitive to the out-of-plane iron motion show more strongly correlated behavior in the stretch factor ($\beta \sim 0.1$)[9] that is more consistent with a hierarchical description of the relaxation process.

On shorter time scales, there is now a growing body of evidence for the importance of collective mode coupling in efficiently directing the reaction forces into functionally relevant motions. By monitoring the acoustic waves generated in the relaxation process of MbCO, it was shown that there are global motions occurring on picosecond time scales.[10] The collective nature of these motions was established by the observed dynamics for an acoustic-like displacement of the protein and the degree of correlation of this displacement with relaxation of the protein near the point of bond dissociation.[11] The two-point spatial correlation in dynamics defines a collective response. Assuming linear response, the protein strain is quadratically proportional to the relaxation energetics and indicates that over 50% of the tertiary relaxation occurs through the displacement of collective modes in the 10 cm^{-1} range. It was argued that this collective mode coupling mechanism is the primary director to the functionally relevant protein motions.[10−12] Since the collective modes in this range are defined by correlated motions of the secondary structure elements, this finding indicates that structure elements such as helices play a critical role in guiding this system through the reaction saddle point of an otherwise very complex surface. This concept is consistent with the analysis of Seno and Go where they found that greater than 60% of the oxy to deoxy structural changes could be reconstituted by the displacement of the lowest frequency collective modes in the 5−12 cm^{-1} range.[13] These workers expounded on the view that the helices behave as rigid structure elements compared to the less rigid loops that act as hinges for directing the motions in such a conserved style. The time scale is not implicit in this work. From the above experimental studies, these collective displacements appear to be occurring predominantly in the inertial phase of the relaxation. Most recently, there has been a much higher resolution determination of the carboxymyoglobin and deoxymyoglobin structures than previously reported.[14] This latter work found an exceptionally strong degree of conservation of the helical sections. The correlation is so strong that it is evident that the helices are simply displaced as a unit (collectively) with heme doming[14] in a process that could be likened to a conformational switch. This new structural information is consistent with the picture drawn from earlier dynamical studies.[10,12]

In this second paper of a two-part series, we present and analyze the OHD TG signals[1] from three related molecules: MbCO, carboxyprotoheme (PHCO), and deoxymyoglobin (deoxyMb). PHCO is the bare ligated heme without a protein wrapper and provides a control system for the electronic-state change of MbCO following photodissociation. DeoxyMb is myoglobin without a ligand, and it serves as a control for relaxation of excess photon energy in the heme protein without any long-lived electronic or structural changes. The work below illustrates that MbCO executes significantly anisotropic motion on picosecond to subpicosecond time scales. The protein effectively changes its shape on time scales consistent with the displacement of collective modes coupled to the heme doming. In essence, we have observed the inertial component to the conformational switching mechanism in directing the reaction forces. This fast initial motion is the dominant anisotropic response within the 0−10 ns dynamic window accessible (rotational diffusion limited) and provides further evidence that the collective mode mechanism is responsible for directing the system response.

II. Sample Preparation and Handling

For the myoglobin samples, horse heart myoglobin from Sigma was mixed with aqueous Tris buffer solution to 1 mM concentration. The solution was centrifuged for 10 min at 10 000 rpm to eliminate clumps of undissolved protein. Then the solution was decanted into the sample cell reservoir to be degassed in situ. The sample was stirred gently for ∼2−4 h while either CO (for MbCO) or N_2 (for deoxyMb) gas was flowed over the sample. After degassing, Fe was reduced from the +3 to +2 oxidation state by adding a 10 times molar excess of sodium dithionate. At all times, the samples were kept on ice to keep the protein from denaturing prematurely and to retard oxidation. After passing through the tubing and sample cell, the sample's temperature in the excited volume was approximately 15 °C. The PHCO samples were handled similarly to MbCO, except that the solvent used for this species was 75% ethylene glycol. This solvent was chosen in order to prevent dimerization of the heme in solution.[15] The UV−vis absorption spectrum of the heme was monitored after preparation to ensure that the sample was in monomeric form.[16]

The protein solution was flowed through the sample cell using a peristaltic pump at a rate fast enough to turn over a sample volume every few laser shots. This prevents accumulation of heat in the bulk solution. At the concentrations used in these experiments, bimolecular recombination to regenerate the fully relaxed protein occurs on submillisecond times.[17] At the 1 kHz laser repetition rate of the experiments, both flowing the sample and recombination enable each laser shot to probe a fully equilibriated sample volume. The sample flask (with 20 mL excess volume) in the ice bath and the peristaltic pump were placed outside the box that enclosed the diffractive optical element (DOE) and sample cell optics. This separate enclosure was necessary in order to eliminate air currents generated both by mechanical motions of the pump and by thermal gradients from the cold ice bath and the pump. The sample was degassed within the reservoir with the cell and tubing attached to remove any residual O_2 inside the closed-loop.

The optical path length through the sample cell was 650 μm, and the transverse dimensions were ∼10 × 5 mm. The optical density at the 400−405 nm excitation wavelengths for most of the 1 mM protein samples was about 2, so that most of the excitation light was absorbed within the first 200 μm of the cell surface. The cell windows were 2 mm thick fused silica, clamped to the stainless steel cell with rubber O-rings.

After ∼200 s of exposure to the excitation beams, it was noticed that a background grating signal from the cell windows

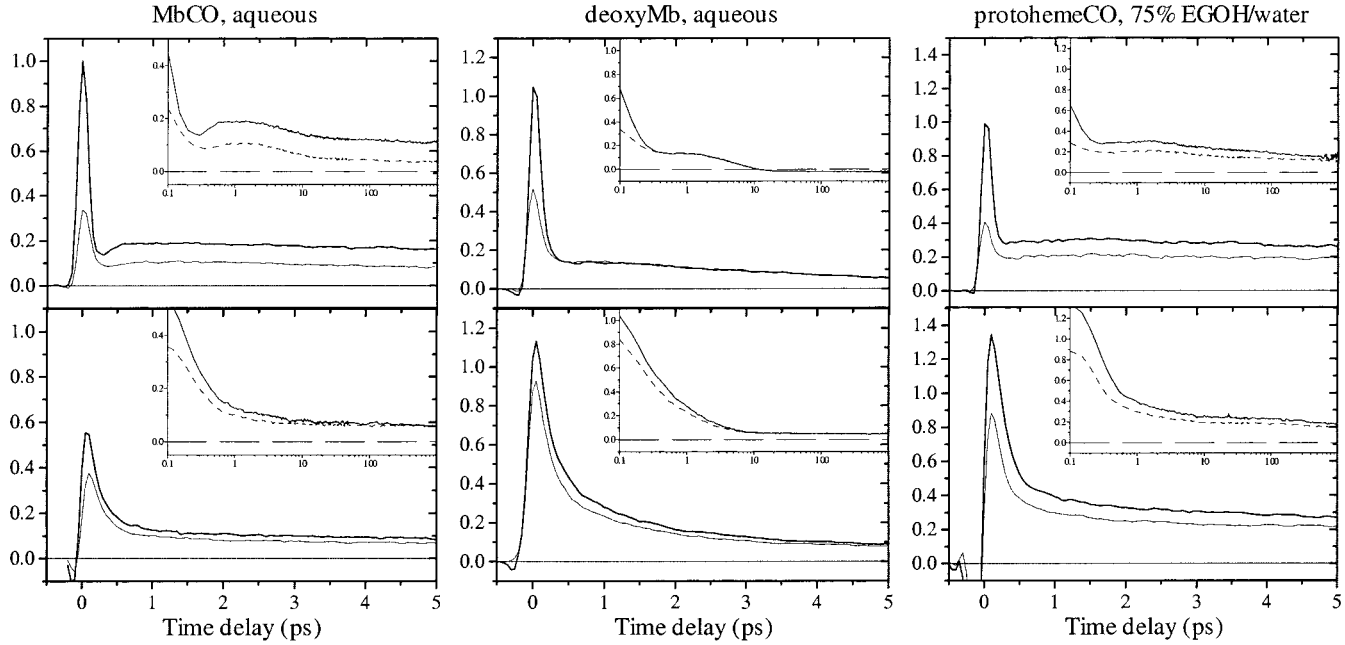

Figure 1. Overview of the OHD grating signals for all three heme species studied using the experimental setup and conditions described in ref 1. The top plots show the real components of $\chi_{1111}(t)$ (solid curves) and $\chi_{1122}(t)$ (dotted curves), and the bottom plots show the corresponding imaginary components. The signal amplitudes between species are arbitrary. The Im components have been multiplied by -1 for a clearer comparison with the Re components (i.e., the absorption increases following photoexcitation in all cases).

began to contribute to the overall signal. This background reduced the S/N but otherwise did not contribute to the recorded dynamics. We observed this effect with just the solvent, but it was more pronounced with protein present. Owing to the high phase stability of the heterodyne setup, even very small quantum yield processes and weak multiphoton processes lead to accumulation of a permanent grating on the windows. This problem was never observed in the absence of the phase-locked excitation pulses. Without phase-locking the random phase shifts between the grating excitation pulses on a shot-to-shot basis causes the optical interference pattern to spatially fluctuate and average out over time. In an analogous fashion, we were able to overcome this problem by simply rocking the cell back and forth along the grating wavevector with an amplitude of $\sim$30 μm to smear out the accumulated pattern. A similar effect has been explored as a mechanism for writing permanent diffractive elements in glasses using high-intensity ultrafast pulses.[18,19] While rocking the cell eliminated the grating pattern, the background scatter was found to increase beyond an acceptable level after 5 min. This effect could arise from a number of photophysical or photochemical processes activated through multiphoton processes that are unavoidable with the high peak power of femtosecond pulses. To completely avoid this problem, the cell was shifted to a fresh spot after every few minutes of exposure to the excitation beams.

III. Results and Discussion

The goal of the heterodyne-detected grating experiments on heme proteins is to separate the dynamics of the excited electronic states from thermal and conformational relaxation. Different physical events can be separated by adjusting experimental parameters such as the protein species, excitation power, and field polarizations. In addition to these experimental parameters, the previously known time dependence of certain features of the grating signals (photoacoustics and hyperpolarizability contributions) can be fitted to the experimental data. The signal contributions from photoacoustic effects are generally of the form $\chi^{\mathrm{sol,s}}[1 + \cos(\omega_{\mathrm{AC}}t)] + \chi^{\mathrm{sol},T}[1 - \cos(\omega_{\mathrm{AC}}t)]$, where $\chi^{\mathrm{sol,s}}$ is the peturbation of the solvent susceptibility owing to changes in the protein strain,[10] $\chi^{\mathrm{sol},T}$ is the change in the solvent susceptibility from changes in the temperature, and ω_{AC} is the acoustic frequency.[20] Impulsive signal contributions that follow the cross-correlation of the applied pulse envelopes (so-called "coherent coupling" artifacts) are ubiquitous in transient grating measurements owing to the third-order electronic hyperpolarizability.[21] These effects are both well understood and can be removed from the data with good precision, simplifying the interpretation of the remaining contributions.

The complete OHD TG signals from each of the species investigated (MbCO, deoxyMb, and PHCO) are shown in Figure 1. The nanosecond acoustic modulation of the data[22] was fit to the appropriate functional form[20] and removed (insets to Figure 1) to simplify inspection of the data out to nanosecond time scales and longer. The acoustics were subtracted so as to keep the amplitude of the Re component near $t = 0$ unchanged. This procedure eliminates the thermal solvent contribution $\chi^{\mathrm{sol},T}$, which is zero at $t = 0$ and peaked at $t = \pi/\omega_{\mathrm{AC}}$.

The Re parts of the grating response contain significant contributions from thermal and conformational protein relaxation in addition to electronic-state relaxation. As a result, the Re part of the time-dependent response is complicated and difficult to immediately interpret. The electronic-state relaxation can be isolated by examining the Im signals, shown in the bottom plots in Figure 1. Conformational relaxation of the protein couples only weakly to the absorptive properties of the heme,[9,23,24] so that to a good approximation the evolution of the Im signals provides information about the excited electronic-state dynamics only.

A. Imaginary Grating Signal. The simplest of the Im grating signals is from deoxyMb, which provides a control for photoexcitation without photodissociation. After absorbing a photon from the excitation field, the heme occupies a very short-lived excited electronic state that exhibits stronger absorbance (in the near-IR) than ground-state Mb. The time dependence of the

excited state(s) can be determined by fitting the imaginary grating signals (equivalent to the pump−probe signal) to a biexponential function convoluted with the pulse cross-correlation.[25−27] A delta-function term is added to the fit function to account for the impulsive third-order hyperpolarizability response.[21] The major signal features are decays of 200 ± 60 fs and 2 ± 0.2 ps, along with a small constant offset whose amplitude is a few percent of the total decay. Each of these features is in reasonable agreement with pump−probe measurements reported by Lim et al.,[24] which have shown that the decay of the pump−probe signal from deoxyMb in the near-IR is predominantly due to relaxation of electronic excited states, with only secondary (although measurable; see below) effects arising from thermal relaxation.

In addition to the grating measurements of the transient absorption in the near-IR, pump−probe studies using a probe wavelength centered at 422 nm were conducted on deoxyMb. This probe wavelength is slightly blue-shifted from the peak of the 25 nm wide Soret band (433 nm) of the unligated heme.[28] The bleaching and recovery of the Soret band absorption provides information complementary to the near-IR absorption dynamics. In the near-IR, there are a number of overlapping transitions that are susceptible to temperature-dependent spectral shifts,[24,28] so that the transient absorption dynamics are sensitive to both electronic-state relaxation as well as thermal relaxation of the heme. In comparison to the near-IR, the Soret transition is extremely strong and less sensitive to temperature,[2,29,30] so that the recovery of the ground-state absorption at 422 nm should provide a clearer probe of the excited electronic-state lifetime, independent of thermal relaxation.

The pump−probe signals at 422 nm from deoxyMb are displayed in Figure 2 along with fits to a biexponential decay function. These results are comparable with those of Petrich et al.,[2] who performed an extensive series of measurements of transient bleaching in the Soret band on a number of heme species. At a probe wavelength of 434 nm, they extracted relaxation time constants of 300 fs and 3.2 ps for deoxyMb. These decay components were taken to represent the decay rates of two distinct excited states of the heme into the unligated ground state, based on their ubiquitous presence in a variety of species at various wavelengths throughout the Soret band. Their 3.2 ps decay rate is in reasonable agreement with the 3.6 ps decay measured here, but the data in Figure 2 do not support the presence of a 300 fs decay component. A possible explanation of this discrepancy is that the earlier studies of Petrich et al.[2] had insufficient time resolution and signal-to-noise (S/N) to resolve the fast 100 fs decay rate. The instrument response for the Soret band studies of Figure 2 was measured to be 75 fs fwhm (55 fs deconvolved pulse widths), which is sufficient to accurately determine decay rates at the 100 fs level. It is possible that the short time constant might be even faster than that measured here, so that the 100 fs rates determined from Figure 2 should be viewed as an upper limit. The other possible difference is the probe wavelength. The difference in probe wavelength is small and both 422 and 434 nm address the Soret band; however, it is possible that an intermediate state may make a larger contribution to the signal at 434 nm than at 422 nm.

The dual-wavelength transient absorption data in Figures 1 and 2 are not sufficient in themselves to deterministically assign physical mechanisms to the decay parameters. A complete set of time- and frequency-resolved transient absorption spectra throughout the near-IR (700−1000 nm) were measured by Lim et al., from which the recovery of the heme electronic ground state was incisively determined to occur with a time constant

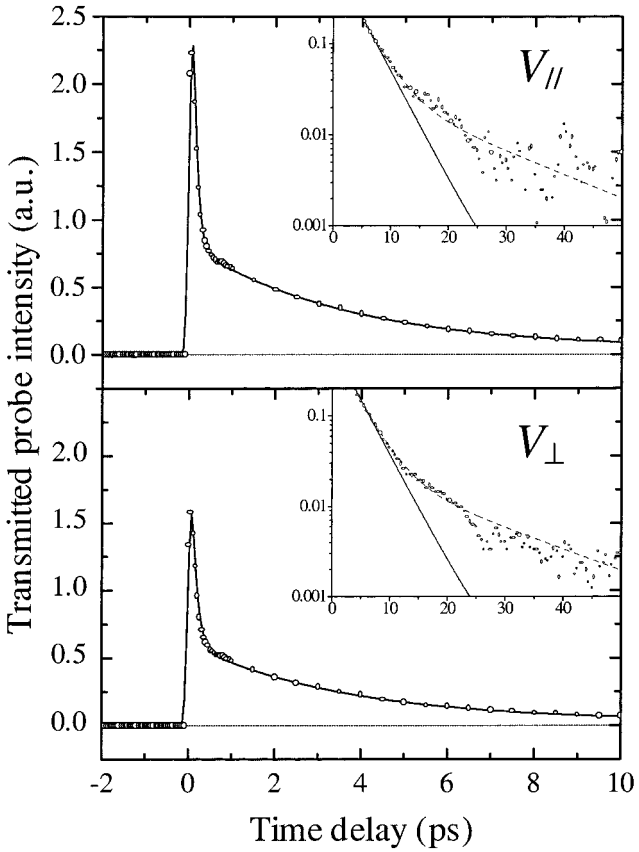

Figure 2. Pump−probe signals (open circles) from deoxyMb at λ = 422 nm for both the excitation and probe pulses. The signals are fit (solid curve) to a biexponential decay convolved with the pump−probe cross-correlation. The resulting decay equations are $V_{||}(t) = 0.82\ \exp(-t/0.10\ \text{ps}) + 0.17\ \exp(-t/3.6\ \text{ps}) + 0.009$ (top data set) and $V_{\perp}(t) = 0.77\ \exp(-t/0.12\ \text{ps}) + 0.17\ \exp(-t/3.6\ \text{ps}) + 0.010$ (bottom data set). These data show the bleaching and recovery of the Soret band, which provides a measure of the time scale for the heme to return to its ground electronic state. Insets: Longer time dynamics with the baseline offset subtracted, showing a very small, isotropic decay. The dotted curves are modifications of the biexponential fits to include an additional ∼16 ps relaxation component (1% of the total relaxation). The best fits for the two faster decay components are not significantly changed when fitting to a triexponential.

of 3.4 ± 0.4 ps.[24] This ground-state recovery manifests itself in the near-IR as an increase in the area of band III, a weak in-plane transition of deoxyMb centered at 760 nm. Simply monitoring the transient absorption at a single wavelength in the near-IR does not provide a clear indication of this ground-state recovery, since the tail of the band III transition overlaps with a number of other distinct spectral features in the near-IR (see Table 1 in ref 1), all of which are sensitive to the heme temperature as well.[24,31] The slow ∼2 ps decay of the transient absorption at 800 nm is thus affected by electronic as well as thermal relaxation. However, the recovery of the strong Soret band absorption in Figure 2 occurs within the experimental uncertainty for the reappearance of the ground state. Since the Soret band is spectrally well isolated from other transitions, it provides a reasonably good probe of the ground-state population. It can thus be inferred from Figure 2 that the heme returns to its equilibrium unligated state with a 3.6 ± 0.2 ps time constant.

Taking a closer look at the decay of the pump−probe signals in the Soret band, it can be seen that in addition to the 100 fs and 3.6 ps decays, there is a small amplitude decay on ∼15 ps time scales. This can be clearly seen from the insets of Figure 2, where the data are plotted on a log scale with the static

component subtracted from both the fit function and the data to clarify the discrepancy between them for $t > 10$ ps. To eliminate this discrepancy, the Soret absorption signals were fit to a triexponential decay function, shown in the insets to Figure 2. The addition of a third relaxation component did not significantly affect the fitted amplitudes or time constants of the first two components owing to the clear separation of time scales between them.[32] The new term was found to have an amplitude of about 1% of the total decay and a time constant of 16 ± 4 ps for both parallel and perpendicular polarizations.

This slow isotropic relaxation most likely reflects the last vestiges of cooling of the heme that occurs through diffusive coupling to the surrounding globin and solvent. At high temperatures the Soret band broadens and red shifts by ~2 nm (~200 K increase).[29] Since the 422 nm probe wavelength is on the blue edge of the Soret transition of deoxyMb, the absorption will be a decreasing function of temperature. The observed decrease in transmission seen in Figure 2 is thus consistent with the effects of thermal relaxation of the hot heme. This decay component was not observed in previous studies that probed at the 434 nm peak of the Soret band of deoxyMb,[2,33] where the signature of heme temperature shifts is expected to be less pronounced.

The 16 ps diffusive thermal relaxation rate measured here is in qualitative agreement with the rates determined from earlier grating studies (<20 ps),[10,34] time-resolved resonance Raman studies (25 ± 14 ps),[35] transient mid-IR absorption studies (~20 ps),[36] and molecular dynamics simulations (20−40 ps).[37] It should be noted that the cooling process is multifaceted, with the bulk of the heme thermal relaxation taking place on faster time scales (~2−6 ps) via coupling to high-frequency collective motions of the globin.[34,35,37,38] The effects of this faster cooling mechanism on the transient absorption signals are obscured by the repopulation of the heme electronic ground state, which takes place on a similar time scale.

Additional information on the structure and dynamics of the excited heme state is provided by the absorption anisotropy for deoxyMb, shown in Figure 3 for both the near-IR and the Soret band. After some fast initial dynamics in the first picosecond, the anisotropy in the Soret band remains approximately constant (to within the S/N) at $r_{lm}(422\text{ nm}) \approx 1/10$. This is the limiting value that is expected for a circular absorber ($\chi_{11} = 0$ and $\chi_{22} = \chi_{33}$ for both the excited and ground states in eq 32 of ref 1) and is consistent with the expected values in the Soret band from Figure 2 of ref 1. The lack of any significant dynamic change in $r_{lm}(422\text{ nm})$ indicates that the final product state has the same symmetry as the initial ground state, providing further evidence that the absorption dynamics correspond to a repopulation of the ground state. Since the bleaching of the Soret transition of deoxyMb at 433 nm overwhelmingly dominates the pump−probe signals, there is no clear indication of the geometry of the excited heme state from the data at $\lambda = 422$ nm.

In the near-IR, the absorption anisotropy is very different than at 422 nm. At 800 nm probe wavelengths, the induced excited-state absorption dominates the bleaching of the ground state, so that $r_{lm}(800\text{ nm})$ contains information on the excited-state symmetry. The initial anisotropy of 0.06 just after $t = 0$ implies that the heme excited-state absorption is strongly polarized within the heme plane. Using the value $r_{lm}(t \sim 1\text{ ps}) = 0.06$ in eq 32 of ref 1 tells us the ratio of in-plane to out-of-plane absorption strength for the intermediate heme excited state is at least 3:1. This ratio is a lower limit—owing to the nonnegligible bleach fraction (estimated ~10% peak) as well as bleach

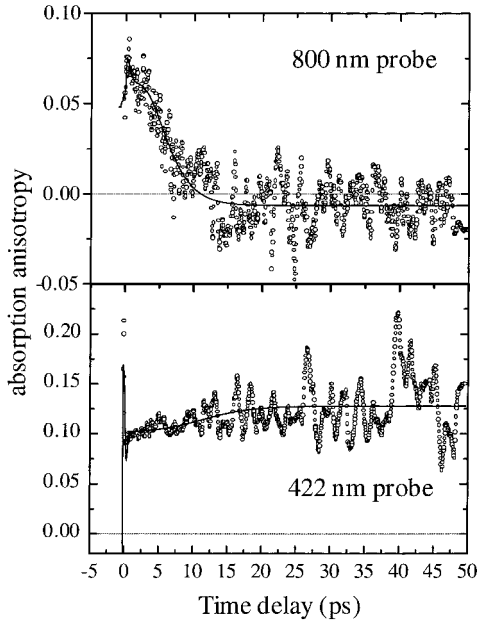

Figure 3. Absorption anisotropy for deoxyMb (open circles) constructed from the data in Figures 1 (800 nm probe, grating geometry) and 2 (422 nm probe, pump−probe geometry). The solid lines show the anisotropy constructed from the fits to the data in Figures 1 and 2. The near-IR absorption anisotropy clearly shows the recovery of the heme ground state.

contributions from the hole burned in the ground state (which has an out-of-plane absorption component at 800 nm); the true anisotropy of the excited state of deoxyMb is likely higher than measured here. This predominantly in-plane polarizability is consistent with an earlier suggestion that the excited-state absorption in the near-IR corresponds to the tail of a higher-energy, in-plane-polarized $\pi \rightarrow \pi^*$ porphyrin transition.[24,29] It is possible that there is some contribution to the decay in the initial anisotropy from cooling of the heme[35] as well.

At $\lambda = 800$ nm, $r_{lm}(t)$ decays from 0.06 to about −0.01 within 10 ps as the heme excited state returns to ground. This final value of -0.01 ± 0.01 is due to the small (about 3%) constant absorptive offset from Figure 1. The small value of the final anisotropy shows that to within the S/N of the measurement, the constant absorbance is isotropic with respect to the heme plane. The long-lived offset in the near-IR absorption was attributed by Lim et al. to two-photon absorption based on its optical power dependence.[24] If the heme absorbs more than one photon, the temperature jump of the heme protein is sufficient to cause the system to sample conformational minima well above the global minimum, where it may become trapped in these higher energy conformations. There is previous evidence for this effect with higher photon energy excitation (355 nm) consistent with this interpretation.[10,34] This conformational change could then lead to a long-lived change in absorption, as observed. The lack of any strongly preferred orientation of the change in the absorption ellipsoid suggests that the constant offset is more likely due to multiphoton heating of the protein than to the reaction $MbO_2 \rightarrow$ deoxyMb, which would indicate oxygen contamination of the sample.

Since the ground state recovers on a multipicosecond time scale, it is not immediately clear what gives rise to the subpicosecond dynamics measured in both the near-IR and in the Soret bands. Lim et al. discounted the possibility of a short-lived electronic state based on the absence of a clear spectral signature in the near-IR.[24] However, the presence of an intermediate electronic state was inferred by the discrepancy in

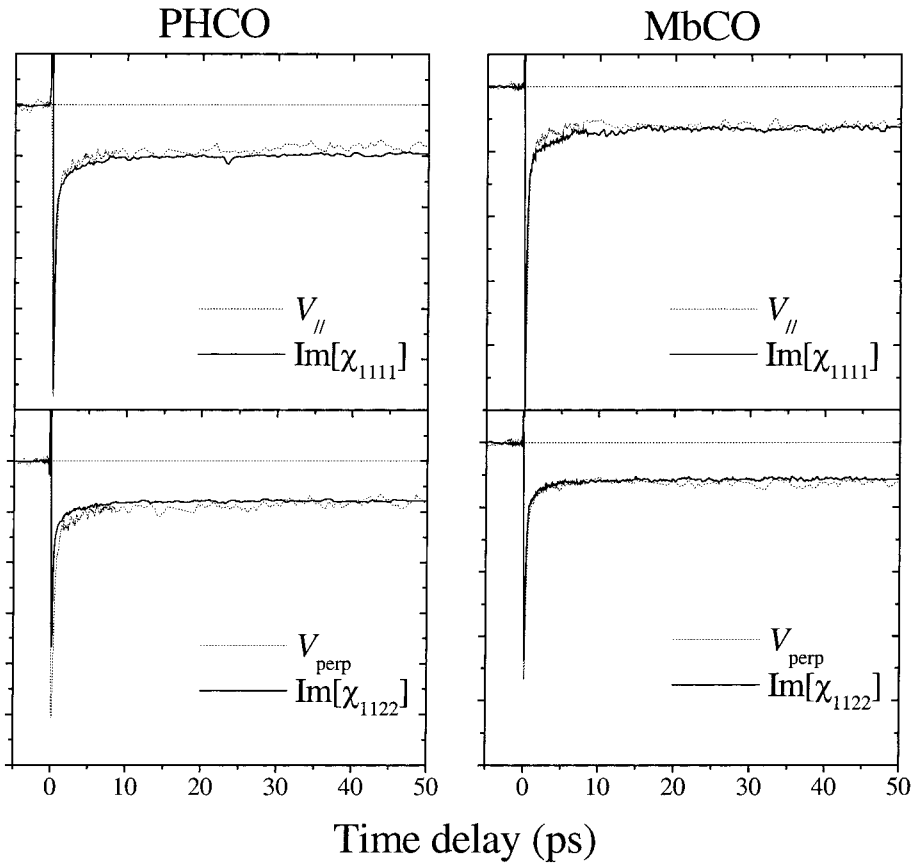

Figure 4. Comparison of the scaled pump−probe signals (dotted curves; $V_{||}$ and $V_{\perp}$) and TG signals (solid curves; Im[χ_{1111}] and Im[χ_{1122}]) for PHCO and MbCO. The agreement between the two different experimental methods shows that they both are proportional to the transient change in absorption of the sample.

the time constants for disappearance of an excited-state feature (∼1.0 ps) and reappearance of the ground-state band III feature (∼3.4 ps). This treatment does not negate the conclusions reached by Petrich et al. from the Soret band dynamics, namely, that upon photoexcitation there are two distinct electronic states that are occupied, with 300 fs and 3.2 ps decay rates back to ground state.[2] Should the 300 fs relaxation rate correspond to the <100 fs decay based on the improved time resolution in the studies presented here, the conflicting pictures set forth in refs 2 and 24 can be reconciled. The <100 fs decay is fast enough that it could indicate the relaxation of a primary photoexcited state, which has been postulated to occur on ∼50 fs time scales.[2,39] If this is the case, the subsequent relaxations observed could correspond to decays of secondary "bottleneck" electronic states. This possibility was noted by Lim et al. but could not be verified by them as their experimental time resolution was limited to ∼300 fs.[24]

Both pump−probe as well as transient grating measurements were performed on the two CO-ligated species, MbCO and PHCO. The results at 800 nm probe wavelengths are compared in Figure 4. It can be seen from this figure that the time dependence of the Im grating signals is very similar to the pump−probe signals for both PHCO and MbCO, except near $t = 0$ where there are large deviations due to the hyperpolarizability contribution. This observation provides a check on the validity of the OHD TG experimental procedure, showing that the measured imaginary component of the grating signal is equivalent to the transient absorption. The signals were fit to biexponential decays as with the deoxyMb data, and the results were found to be consistent with earlier pump−probe studies.[23] The gross features of the signals at 800 nm probe wavelengths are quite similar between PHCO and MbCO. There is a large constant offset at long time delays due to the difference in absorption of the ligated and deligated species. The dynamics at 800 nm are well-described by a fast 200−350 fs decay component, followed by a slower 2−4 ps decay. The small differences in the time constants extracted from these data can be attributed to the slightly different beam geometries and to uncertainties in fitting the large instantaneous contribution to the TG signals. In all cases, the absorption anisotropy is approximately constant after $t = 5$ ps at $r_{Im}(800\ nm) = 0.04 \pm 0.05$. This is in agreement with the expected limiting values in Figure 2 of ref 1 determined from the equilibrium difference spectra.

If PHCO is a valid control for the electronic-state relaxation of MbCO, the Im components of the grating signals should be virtually identical between the two species. This comparison is made in the left-hand side of Figure 5, which shows the difference of the Im grating signals from MbCO and PHCO (with the PHCO data scaled by a constant factor). The only significant difference between the two signals occurs near $t = 0$ and approximately follows the pulse cross-correlation, suggesting that it corresponds to the instantaneous contribution to the grating signals. The relative magnitude of the instantaneous contribution with respect to the molecular responses could change on the basis of a number of experimental issues. For example, small differences in the pulse widths between collecting data sets could change the peak intensity at the sample, increasing the impulsive response while not affecting the amplitude of the time-delayed response. If the excitation fluence were high enough to dissociate a macroscopic fraction of the sample, then changes in the 400 nm pulse energy would cause

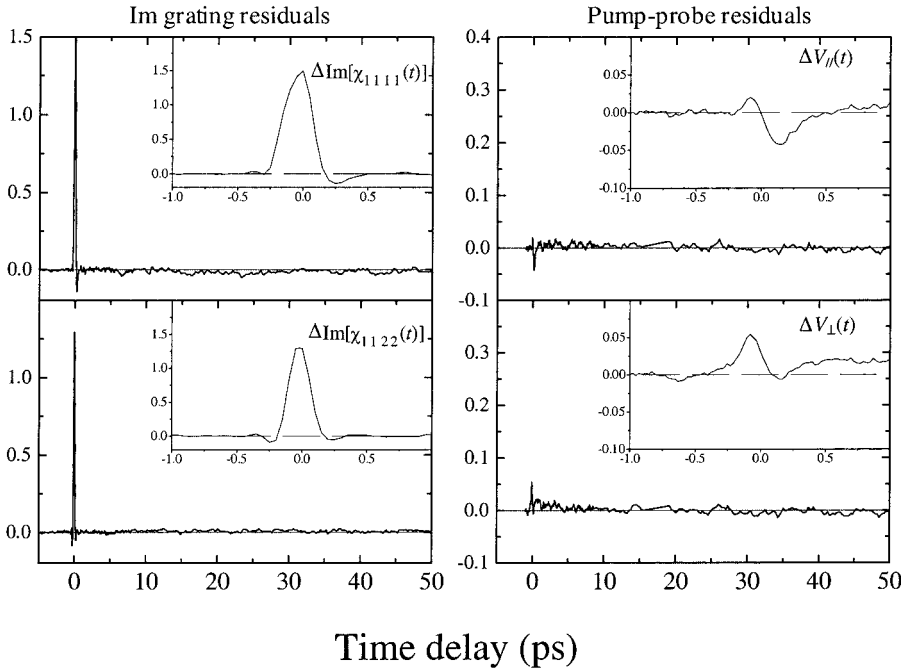

Figure 5. Difference between the PHCO and MbCO absorptive dynamics: (left) imaginary grating signals; (right) pump−probe signals. The residuals for the TG signals approximately follow the pulse cross-correlation, indicating the only major difference is in the impulsive contribution to the signals. For the pump−probe case the residuals are much lower owing to the smaller impulsive component in this experiment. These results show that the electronic-state dynamics are very similar between the two species, so that PHCO should be a reasonable control for the electronic-state dynamics of MbCO.

TABLE 1: Fit Parameters of the Re Grating Signals Fitted to the Convolution of the Pump−Probe Cross-Correlation with a Triexponential Decay of the Form $P_0 + \sum_i P_i \exp(-t/T_i)$, Where $i = 1, 2, 3$[a]

species/element	P_0	P_1	T_1 (ps)	P_2	T_2 (ps)	P_3	T_3 (ps)	P_δ
MbCO Re[χ_{1111}]	0.061	−0.186	0.20	0.359	0.09	0.04	7.1	0.862
MbCO Re[χ_{1122}]	0.023	0.084	0.31	0.189	0.13	0.039	6.1	0.225
PHCO Re[χ_{1111}]	0.105	−0.27	0.30	0.268	0.27	0.051	8.5	0.926
PHCO Re[χ_{1122}]	0.072	−0.327	0.24	0.384	0.20	0.040	7.7	0.264
deoxyMb Re[χ_{1111}]	−0.009	−0.05	0.42	0.701	0.09	0.098	5.0	0.546
deoxyMb Re[χ_{1122}]	−0.008	−0.216	0.29	0.294	0.22	0.096	5.1	0.414

[a] A hyperpolarizability response $P_\delta\delta(t)$ is also included in the decay function. Since the dynamics at short times are clearly nonexponential, the uncertainties on the fast decay components P_1 and P_2 are on the order of 100%. These two fast components simply provide a very rough parametrization of the dynamics and are not expected to directly relate to underlying physical processes. The uncertainties on the other decay times and amplitudes are generally about 10%. The relative scaling between species is arbitrary, but the fit parameters for each species are on the same scale.

larger changes in the instantaneous response than in the saturated molecular response. Additionally, since the 400 nm excitation wavelength is absorbed more strongly by PHCO than by MbCO,[16,28] the effective grating thickness and pulse overlap geometry is different for the two cases. This would be expected to have a strong effect on the instantaneous contribution, which arises from interactions throughout the window thickness as well as in the sample itself. Finally, it is likely that the absolute magnitude of the change in absorption at 800 nm between the ligated and deligated forms is different for the PHCO and MbCO species. Since the instantaneous response has nonnegligible contributions from the windows and solvent, this will obviously result in different ratios of the instantaneous/molecular contributions between PHCO and MbCO.

The similarity of the electronic-state dynamics between PHCO and MbCO can be seen more clearly from a comparison of the pump−probe signals, shown on the right-hand side of Figure 5. The pump−probe signals are less susceptible to the impulsive nonresonant contributions that dominate the initial OHD TG signals. The only significant difference between the two species occurs within ∼300 fs about $t = 0$. This constitutes less than 20% of the pump−probe signal and is again most likely due to a small instantaneous window/solvent contribution. These results show that the electronic-state evolution of PHCO following photodissociation provides a reasonably good control for that of MbCO for $t > 300$ fs. This means the real parts of the PHCO and MbCO signals can be directly compared to isolate dynamics due to thermal and conformational relaxations of the globin.

B. Real Parts. It is expected that changes in the temperature and geometry of the globin will manifest themselves more strongly in the Re component of the grating signals than the Im component. From Figure 1 it is clear that for all species, the Re and Im signals exhibit very different dynamics. A triexponential fit to the Re grating signals for PHCO, deoxyMb, and MbCO generates the fit parameters listed in Table 1. The general features of these signals are (1) a large spike near $t = 0$ that follows the pulse correlation and is most probably a hyperpolarizability contribution, (2) a small delayed rise in the signal ∼200−300 fs after $t = 0$, (3) a slower 5−8 ps decay, and (4) a constant offset. The triexponential form provides a somewhat better fit to the data than a biexponential, but it is not clear whether the additional relaxation component is physically meaningful. This additional component P_3 is needed in order to cancel the negative amplitude component P_1 near $t = 0$ to avoid distorting the falling edge of the spike. The small difference in the time constants of the P_1 and P_3 components

results in a slowly rising signal, as observed. However, it is more likely that the initial signal dynamics are nonexponential. Close inspection of the fits reveals that the Re components cannot be perfectly fit with a multiexponential decay. The time-delayed rise in the signal after about 300 fs is clearly nonexponential—the triexponential fits exhibit systematically slower dynamics that start too close to $t = 0$. Since this feature is present for all species studied, it is possible that it may correspond to a nonresonant, Raman-active nuclear contribution from the solvent, sample cell window, or the heme itself. If Raman effects contribute, it is doubtful that they arise from the glass windows of the sample cell since the peak amplitudes of the OHD time-delayed nuclear and instantaneous electronic $\chi^{(3)}$ responses in glasses have been found to have a ratio of less than 1/200,[40] far too small to explain the observed rise in the TG signals. Similarly, Raman contributions from the solvent can be ruled out since the ratio of nuclear:electronic signal contributions for water is only about 1/50, and the dephasing time is much too fast to yield a ~1 ps rise, as observed here.[41] In addition, since the 400 nm excitation pulses are nearly on-resonance with the extremely strong Soret transitions, the effective cross-section for processes driven by linear absorption (i.e., triggered by photodissociation) is expected to be far larger than the Raman cross-section. Thus, a more likely explanation is that the ~1 ps feature may be due to heating of the heme as the excess photon energy is thermalized. Additional evidence supporting this interpretation is provided by the power-dependent results below.

The longer time scale decay in the signals is somewhat more interesting. From the previous section, it was found that the electronic-state evolution is virtually complete after $t = 5$ ps; thus, this signal component is most likely not due to decay of an excited electronic state. Since it is present within all species studied, it is possible that this corresponds to thermal relaxation of the initially hot heme. From Table 1, it can be seen that the T_3 decay component is slightly faster for deoxyMb and MbCO (5−7 ps) than for PHCO (8−9 ps). This is consistent with the known dynamics of the heme cooling: the heme relaxes to thermal equilibrium with the surrounding protein and solvent both through normal diffusive processes and through coupling to low-frequency collective modes of the protein. It is thought from earlier studies that thermal relaxation via the collective modes of the globin is both the faster and more efficient cooling channel,[34] with up to 90% of the excess heme thermal energy routed this way.[35] The time scale for thermal relaxation via collective motions has been estimated to be between 1 and 7 ps.[35−37] The interpretation of the T_3 decay component as reflecting the cooling of the heme is consistent with these earlier observations. The observed rate T_3 is noticeably slower in PHCO, where the globin is not present to efficiently channel thermal energy into collective mechanical motions.

DeoxyMb provides the clearest picture of thermal decay in the protein, since there is no long-lived change in the electronic-state configuration to obscure the grating signals. The phase anisotropy constructed from the Re deoxyMb grating signals of Figure 1 is shown in Figure 6. Clearly, all the dynamics after the initial spike at $t = 0$ are completely isotropic. This is as one might expect for diffusive thermal relaxation in the globin, where a large number of vibrational modes of the protein are populated thermally. These modes are evenly distributed throughout the highly folded, helical protein structure, with no preferred orientation; i.e., vibrational modes are not preferentially populated on the basis of their orientation with respect to the heme plane. The seemingly abrupt change in the value of

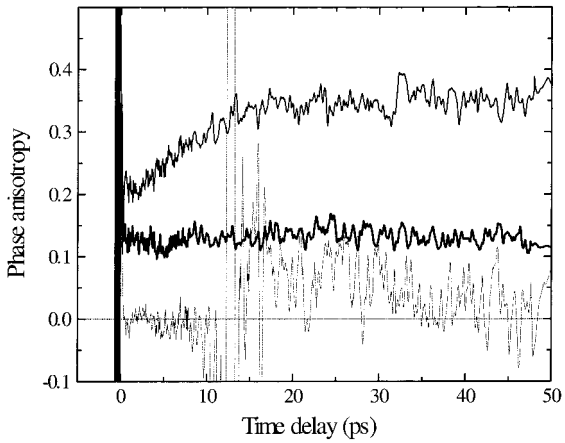

Figure 6. Phase anisotropy of MbCO (solid curve), PHCO (heavy solid curve), and deoxyMb (dotted curve) constructed from the Re grating signals of Figure 1.

r_{Re} at $t = 15$ ps occurs when the contribution from the hot heme/protein has decayed almost to 0 and the small contribution from the long-lived, negative offset in the deoxyMb Re signal becomes dominant (see Figure 1). On the basis of the lack of any significant phase or absorption anisotropy at long times [$r_{Re}(t > 20$ ps) ≈ 0 to within the S/N in Figure 6, and $r_{Im}(t > 20$ ps) $= -0.01 \pm 0.01$ in Figure 3], it is likely that this offset arises from multiphoton excitation populating higher energy components in the conformational distribution, with accompanying small shifts in the spectra, as discussed above.

The phase anisotropies of PHCO and MbCO are also shown in Figure 6. The phase anisotropy of PHCO is virtually constant at $r_{Re} = 0.13 \pm 0.02$. This is consistent with the expected long-time limiting value for the anisotropy of the dipole transition of MbCO displayed in Figure 2 of ref 1. In contrast to the behavior of PHCO, the phase anisotropy of MbCO is much larger than can be attributed to the change in the electronic state, with $r_{Re} = 0.35 \pm 0.03$ after $t = 20$ ps. The initial smaller value of the phase anisotropy at short times is due to the isotropic signal contributions from the hot protein, which decay to nearly 0 after ~15 ps.

It could be possible that this large final value of the phase anisotropy of MbCO is simply due to addition of a large negative isotropic signal to the positive anisotropic signal contributions from the electronic-state change. It was shown in Figure 5 that the electronic-state evolution is nearly identical between PHCO and MbCO. Since PHCO does not have the globin present, it is a good control for the electronic-state relaxation of the heme. Accordingly, the Re grating signals of PHCO and MbCO can be compared to find the dynamic response that arises from the protein part of the molecule. In Figure 7, the Re grating signal of PHCO is subtracted from the MbCO signal, with the scaling determined by the Im grating signals of Figure 5. The remaining signal components in Figure 7 should be predominantly due to protein relaxation dynamics. Clearly, there is a very large anisotropic contribution to the real component of the MbCO signal that does not arise from electronic-state dynamics. This anisotropy is most likely indicative of the highly anisotropic change in the protein conformation upon photodissociation.

A caveat regarding the method used for subtraction of the electronic-state contributions to the Re grating signals should be mentioned here. This procedure is based on the observation that the time-dependent Im grating signals of MbCO and PHCO exhibit virtually identical dynamics at a probe wavelength of 800 nm. This observation is not sufficient to argue that the corresponding phase evolution of the electronic-state change is

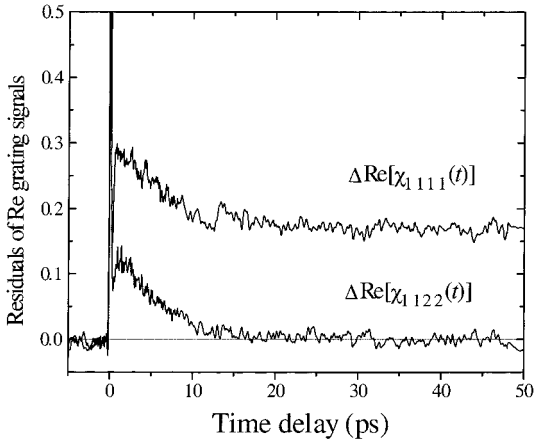

Figure 7. Difference between the real grating signals from MbCO and PHCO. The relative scaling factor between the two species is the same as that used in Figure 5 to eliminate the difference between the Im grating signals. Clearly, there is a large anisotropic contribution to the real component of the MbCO signal that does not arise from electronic-state dynamics.

identical between PHCO and MbCO. To make this connection rigorously, it is necessary to show that the absorptive dynamics are the same between PHCO and MbCO at all probe wavelengths, so that eq 35 of ref 1 for the time-dependent Kramers−Kronig (KK) relationship between the Re and Im signals is identical for the two species. Unfortunately, the transient absorption dynamics of the two species are not the same, as can be seen by comparing the frequency-resolved pump−probe signals in the Soret band. While the spectral shapes and time dependence are similar, for PHCO the Soret band and the associated transient bleaching/absorption are blue shifted by ∼15 nm from those of MbCO.[16,28] However, probe wavelengths in the near-IR are far enough off-resonance from the strong Soret and Q-band transitions of the heme that the value of the KK integral over these transistions will not be greatly changed by a ∼15 nm shift of the line centers. Thus, despite the different absorption dynamics between PHCO and MbCO, at 800 nm probe wavelengths a KK connection between the Re and Im dynamics of the two species should be a reasonable approximation.

The nonelectronic contributions to the grating signals shown in Figure 7 contain information primarily about the solvent and the globin part of the protein [$\Delta\chi^{sol}$ and χ_{ii}^{glob} in eqs 21 and 22 of ref 1]. To relate these signals more directly to the geometry of the protein, they can be decomposed into effective changes in the index of refraction along directions in the heme plane and along the heme normal as per eq 28 of ref 1. This decomposition is shown in Figure 8. These residual index changes can be analyzed in terms of their functional dependence on the molecular contributions to the grating signals. From eq 14 of ref 1, the change in susceptibility of a protein molecule upon photodissociation is

$$\Delta\chi_{ij} = \Delta\chi^{sol}\delta_{ij} + \chi_{ij}^{e}(\omega_{pr}) - \chi_{ij}^{g}(\omega_{pr}) + \chi_{ij}^{glob} \qquad (1)$$

Here the molecular susceptibility change $\Delta\chi$ is written in the basis relative to the heme axes, so that the laboratory coordinates Ω do not contribute. Since the thermally driven photoacoustics make essentially no contribution to the signal within the first 50 ps, the term $\Delta\chi^{sol}$ in eq 1 contains only the contribution from the structure change $\Delta\chi^{sol,s}$. The contribution $\chi_{ij}^{e}(\omega_{pr}) - \chi_{ij}^{g}(\omega_{pr})$ from the electronic-state change is eliminated through subtraction of the PHCO response. Inserting the remaining terms from

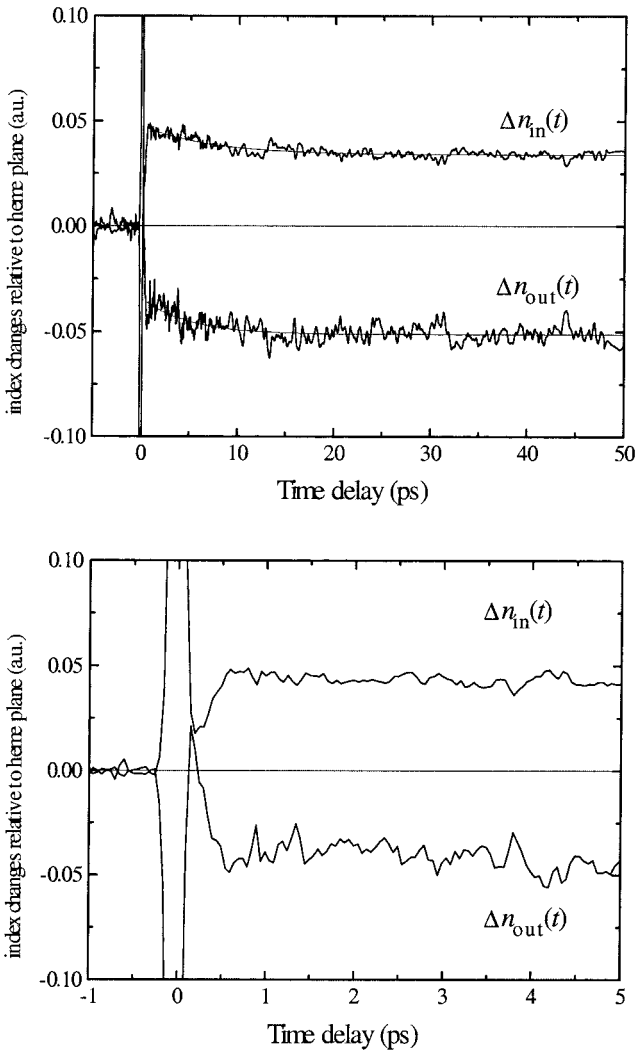

Figure 8. Nonelectronic contributions to the in-plane and out-of-plane index changes relative to the heme plane for MbCO. These traces are constructed from the residuals of the Re grating signals shown in Figure 7 and show the very anisotropic contributions of protein strain to the observed signals. The dotted curves in the top plot are single-exponential fits to the data for $t > 1$ ps, with time constants of 7.1 ± 2 and 4.9 ± 2 ps for the in-plane and out-of-plane decays, respectively. The initial development of the in-plane and out-of-plane index changes on a 300 fs time scale is suggestive of the possible time scale over which global strain may develop in the protein.

eq 1 into eq 25 of ref 1, the index changes displayed in Figure 8 can be written,

$$\Delta n_{in} = \Delta\chi^{sol,s} + (\Delta\chi_{22}^{glob} + \Delta\chi_{33}^{glob})/2$$
$$\Delta n_{out} = \Delta\chi^{sol,s} + \Delta\chi_{11}^{glob} \qquad (2)$$

It can be seen from eq 2 that both the in-plane and out-of-plane index changes contain equal contributions from the solvent, as expected since the solvent response is isotropic. The remaining contribution is from the globin, along the heme normal for $\Delta n_{out}(t)$ and averaged over the two in-plane directions for $\Delta n_{in}(t)$. Clearly, every microscopic contribution to the index changes in Figure 8 arises from conformational relaxation of the protein, either through a direct interaction with the protein [$\Delta\chi^{glob}(t)$] or through the effect on the solvent density ($\Delta\chi^{sol,s}$). It is apparent from Figure 8 that the globin contribution is highly anisotropic, since the in-plane and out-of-plane index changes are positive and negative, respectively. Given this observation,

is it possible to infer the signs of the globin contributions in-plane and out-of-plane? From earlier studies of the acoustics generated by photodissociation of MbCO, the initial solvent contribution to the change in index $\chi^{sol,s}$ is opposite the sign of the thermally launched acoustic wave, $\chi^{sol,T}$.[10,11] This assignment was based on the comparison of different heme and heme proteins with nearly identical optical properties, as well as absolute diffraction efficiencies at different probe wavelengths that indicate the protein strain dynamics were adding to the underlying electronic phase grating term (increased diffraction). The sign of the thermal grating is well-known. Heating the solvent leads to thermal expansion and a decrease (negative change) in the solvent density, so that the associated index change $\chi^{sol,T} < 0$, implying $\chi^{sol,s} > 0$. With this information, $\chi^{sol,s} > 0$ in eq 2 implies $\chi_{11}^{glob} < 0$ in order for the sign of the net out-of-plane index change Δn_{out} to be negative, as seen in Figure 8.

The globin contribution can be interpreted as being proportional to strain (relative atomic displacements) induced in the protein. For any material, the sign of the molecular strain is opposite the sign of the index change; positive strain corresponds to material expansion, with a concurrent decrease in both density and the index of refraction.[11] So it can be inferred from Figure 8 that the protein is expanding along the direction perpendicular to the heme plane. However, the sign of the net strain within the plane of the heme cannot be definitively determined from Figure 8 and eq 2. The observed sign of $\Delta n_{in} > 0$ could be attributed to the positive contribution $\chi^{sol,s}$ from the solvent as discussed above. It is possible that $\chi_{22}^{glob} + \chi_{33}^{glob} > 0$, so that the protein may be contracting within the heme plane with an overall magnitude that is less than the out-of-plane expansion in order to conserve the net volume occupied by the protein. This would make intuitive sense—if stress is applied to an elastic medium along one direction, the resulting strain along the direction in which the stress is applied would be opposite the sign of the induced strain along the perpendicular directions in order to keep the density constant. But since there is a nonzero change in the volume occupied by the globin,[10] the possibility that the protein may be expanding within the heme plane as well as perpendicular to it cannot be ruled out definitively. Nevertheless, even if the in-plane and out-of-plane strains have the same signs, their magnitudes are greatly different. Thus, it can be concluded that the shape of the protein is changing on extremely fast ($<$500 fs) time scales.

The initial development of $\Delta n_{in}(t)$ and $\Delta n_{out}(t)$ in Figure 8 can be seen to be substantially complete within ~500 fs after photodissociation. The initial rise in Figure 8 is suggestive of the time scale for global strain to develop in the protein. However, this initial rise should be viewed cautiously, since the electronic-state dynamics of PHCO and MbCO do not precisely cancel within a ~0.5 ps window surrounding $t = 0$ (see Figure 5). At any rate, after this initial rise the in-plane and out-of-plane index changes are fully formed. This implies that the mechanical modes of the protein involved in the conformation change are in the range of a few 10's of cm^{-1}. This frequency range corresponds to collective motions of large portions of the globin. The lack of any substantial oscillations in the index change shows that these collective modes are strongly damped—the protein very quickly relaxes to its deligated configuration.

The only remaining dynamic contribution after the first 500 fs is well described by a 5−7 ps decay of approximately the same amplitude for both the in-plane and out-of-plane index changes, as shown by the fits in Figure 8. This is very similar to the dynamics seen in deoxyMb, suggesting that this remaining contribution arises from isotropic diffusive cooling of the heme protein.

These results should be compared to previous studies that employed direct-detected grating methods.[10,11,34,42,43] The conformational dynamics revealed through heterodyne detection of the grating signals have now been fully resolved with 100 fs time resolution. The improved time resolution of the current studies over previous efforts is in part due to the use of shorter pulses[10,42,43] and in part due to the enhanced information content of the OHD signals over the previous direct-detected studies.[11] It was inferred earlier on the basis of fits for the phase shifts of the generated photoacoustics and fits to residuals between MbCO and heme-octapeptide (a control for the electronic contributions similar to PHCO used above) that the protein conformational relaxation takes place with a time constant of ~1−2 ps.[11] A relaxation component in this range is not observed in the present work. Error estimates were not explicitly reported in the previous work for the fitted time constant of the protein-generated acoustics. From inspection of the reported data, the calculated phase shift for an instantaneously driven acoustic wave provides a comparable fit to the data (Figure 4 of Deak et al.).[11] Thus, the results presented here are consistent with the data presented by Deak et al. The argument presented in ref 11 for a 1−2 ps conformational relaxation time was based primarily on the observation of a ~1 ps dynamic relaxation component to the difference between the direct-detected grating signals from MbCO and heme-octapeptide. This result from ref 11 is similar to that constructed in Figure 7, except that since the grating signals were quadratic in the nonlinear polarization, cross-terms between various relaxation components prevented complete removal of electronic-state dynamic contributions in this earlier work. The ~1 ps relaxation of ref 11 is quite similar to the delayed rise observed in the residuals of Figure 7. However, the more fundamental quantities with regard to the underlying molecular dynamics are the non-electronic-state contributions to the in-plane and out-of-plane components of the index ellipsoid, shown in Figures 8 and 9. At low power, there is very little evolution of these index changes after the first few hundred femtoseconds (Figure 8). It is only at higher pump powers (Figure 9) where there appears a ~1 ps component to these index changes (vide infra). The slightly higher bleach fraction in this earlier work and inability to separate the different components to the signal likely account for the noted difference. These differences are within confidence limits such that the studies are in relatively good agreement.

C. Pump Power Dependence. The grating signals are expected to vary as a function of the applied excitation intensity. Obviously, increasing the pump power will increase the number of photodissociated molecules and thus lead to an increase in the overall signal amplitudes. But, in addition to this, when the pump power becomes large enough that a significant fraction of the molecules in the illuminated volume are excited, the shape of the signals can change as well. Specifically, multiphoton absorption leads to substantially more excess energy in the protein and may access other relaxation pathways. The experiment on MbCO was repeated at a higher pump power (12 μJ rather than 4 μJ, corresponding to a peak bleach fraction of 30% rather than 10%). It was difficult to go to much higher excitation levels than this, as higher bleach factors wash out any of the details pertaining to the anisotropic response of interest.

The OHD grating signals from MbCO at this higher excitation energy of 12 μJ (3 times the level used normally) are shown in

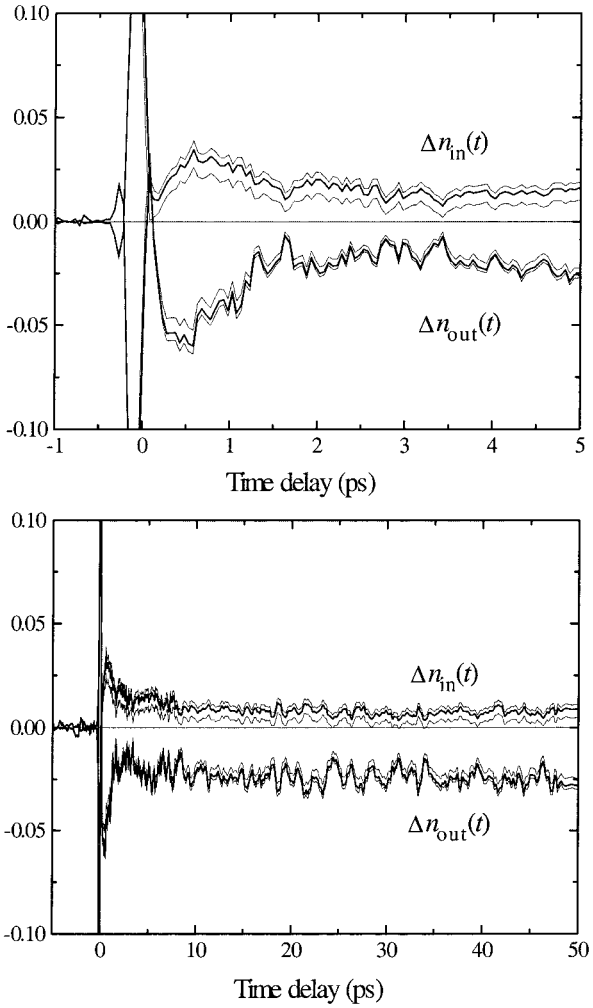

Figure 9. Nonelectronic contributions to the in-plane and out-of-plane index changes for MbCO at $U_{ex} = 12$ μJ. The dotted curves indicate the uncertainties in this construction owing to power saturation of the absorption anisotropy.

Figure 10. The nonelectronic contributions to the in-plane and out-of-plane index changes constructed in the same manner as for the low-power data are shown in Figure 9. There is some degree of ambiguity in this construction owing to the saturation of the absorption anisotropy at high powers—the correct scaling factor to subtract the PHCO response from the MbCO response is less certain. The smaller absorption anisotropy at high power can be seen by the incomplete cancelation of the Im grating signals at long times ($t > 5$ ps) in Figure 11. The effects of this scaling uncertainty on the nonelectronic contributions to the in-plane and out-of-plane index changes are indicated by the dotted curves in Figure 9.

As in the low power case of Figure 8, the initial dynamic evolution of the index changes in Figure 9 is dominated by a residual hyperpolarizability contribution at $t = 0$, followed by a fast ~500 fs rise of the index changes as described above. There is also an additional ~1 ps relaxation component in Figure 9 that is not present at low powers. Because the PHCO and MbCO data were collected under different excitation conditions, it is not immediately clear whether the ~1 ps dynamic contribution to the index changes indicates different underlying physics or whether it is merely an artifact of incomplete cancelation of the electronic-state dynamics. The question can be addressed by inspection of the residuals of the Im grating signals between MbCO at 12 μJ and PHCO at 4 μJ, shown in Figure 11. The scaling uncertainties are also shown clearly in this figure. After the first ~0.5 ps, the Im signal dynamics from the two traces cancel each other reasonably accurately. This suggests that the electronic-state dynamics are not strongly affected by the higher pump power, and the ~1 ps dynamic evolution of the in-plane and out-of-plane index changes observed in Figure 9 is due to a nonelectronic effect.

The most straightforward explanation for this decay component is that it is due to multiphoton excitation of MbCO. After absorption of the first photon, subsequent absorption events will only contribute to processes such as heating of the heme and excitation of Raman-active modes. One explanation for the picosecond dynamic in Figure 9 is that it may indicate the phase effects of increased heating of the heme. If this were the case, the fast 1 ps time scale of the index evolution suggests that the thermal decay channel is strongly coupled to collective modes of the globin—relaxation of the excess photon energy via thermal diffusion would be expected to occur on approximately 1 order of magnitude slower (~5−20 ps) time scales.[35−38] It is interesting that no ~10 ps decay component is observed in Figure 9. This implies that the amplitude of the diffusive thermal relaxation channel is not increased nearly as much as the amplitude of the collective mode relaxation channel. This observation is consistent with the physics underlying the collective mode relaxation mechanism. The rate of energy transfer between modes depends on the nonlinear coupling between them.[44] At higher temperatures, the nuclei in the protein oscillate further from their equilibrium positions than at lower temperatures, so that modes sample more of the anharmonic part of the potential surface and are in effect more strongly coupled. Thus, as the temperature increases, it is expected that a greater fraction of the excess thermal energy will be transmitted from the protein to the solvent via the collective modes rather than through diffusion processes, as suggested by the fast dynamic contribution to Figure 9.

It can also be seen from Figure 9 that the magnitudes of both the in-plane and out-of-plane index changes are much smaller than in the low-power case. (The magnitudes of the index changes in Figures 8 and 9 can be directly compared since they are both scaled relative to the same PHCO data set.) This decrease in the magnitudes of Δn_{in} and Δn_{out} is a clear-cut consequence of the large bleach fraction. As the pump power is increased a larger fraction of unfavorably aligned molecules is excited, and the difference between the parallel and perpendicular signals $\chi^{(3)}_{1111}(t)$ and $\chi^{(3)}_{1122}(t)$ becomes less. This in turn causes the constructed Δn_{in} and Δn_{out} to become less dissimilar, as observed in Figure 9. This effect can also be seen in the power dependence of the phase and absorption anisotropies at high power, shown in Figure 12. The decreases in $r_{Im}(t)$ and $r_{Re}(t)$ as the pump power is increased is consistent with the expected bleaching behavior.

It is interesting to compare the dynamics of the phase anisotropy of MbCO at high power from Figure 12 to those at low power in Figure 6. Qualitatively, the two traces exhibit similar features, with an initial spike near $t = 0$ owing to the hyperpolarizability contribution followed by a ~15 ps rise to the final value near 0.35. The 15 ps rise can be primarily attributed to the diffusive thermalization of the excess photon energy, as discussed earlier. Diffusive cooling of the heme and protein results in an isotropic decrease in both $\mathrm{Re}[\chi_{1111}(t)]$ and $\mathrm{Re}[\chi_{1122}(t)]$ (the ~5−10 ps decays in Figures 1 and 10), with a concurrent increase in the anisotropy. The clearest power-dependent feature seen by comparing Figures 6 and 12 is the initial spike in the anisotropy peaked near $t = 500$ fs, when thermal activation of collective motions of the protein is most

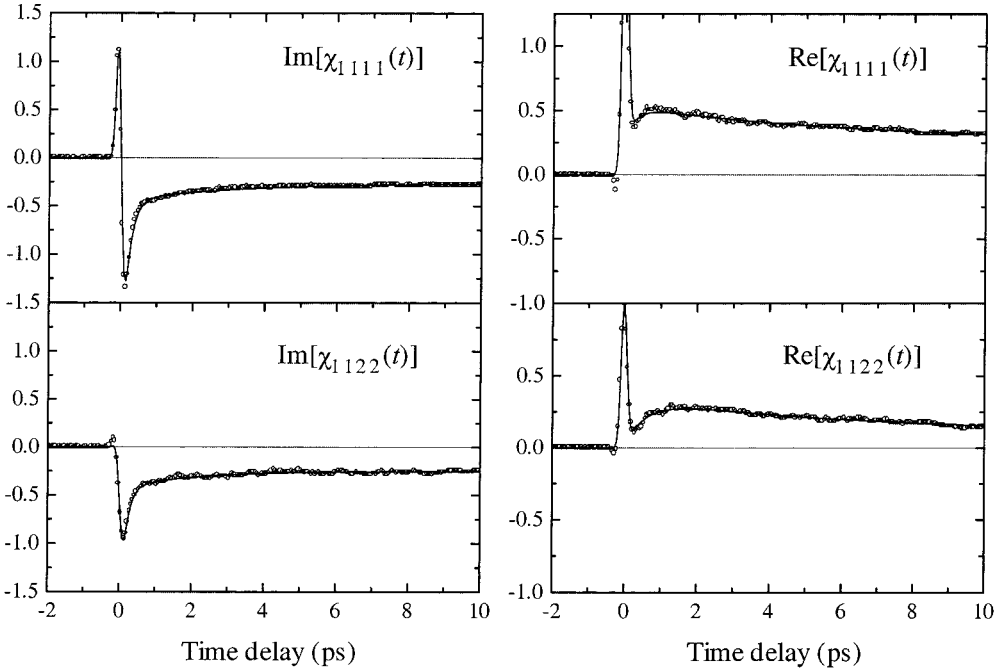

Figure 10. OHD TG grating signals from aqueous MbCO at $U_{ex} = 12\ \mu J$, about 3 times the usual excitation energy. In comparison to the low power data in Figure 1, the Im grating signals are relatively unchanged, but the Re signals exhibit a more pronounced nonexponential rise in the first ~1 ps. This may point toward an increased involvement of collective motions of the globin in transmitting thermal energy from the heme to the solvent at high temperatures.

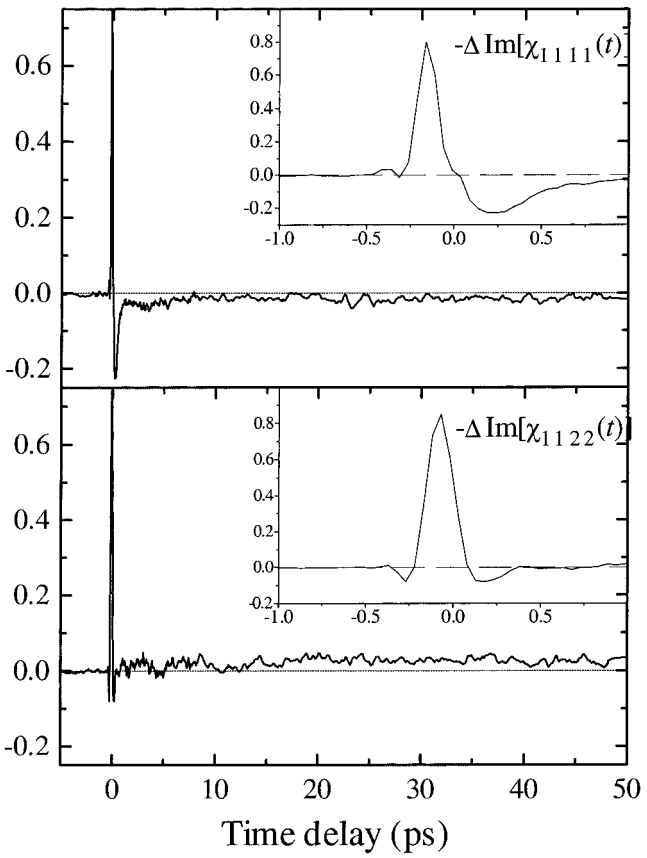

Figure 11. Residuals for Im grating signals of PHCO at $U_{ex} = 4\ \mu J$ and MbCO at $U_{ex} = 12\ \mu J$. The electronic-state dynamics more or less cancel outside the 0.5 ps window surrounding $t = 0$ except for a small remaining offset that is due to power saturation of the anisotropy.

strongly evident. The increased phase anisotropy of MbCO at $t = 500$ fs at higher powers is completely opposite the expected bleaching behavior. This clearly shows that there is an additional physical mechanism contributing to the grating signals at high powers that is less prevalent at low powers. It has already been shown that the protein strain is highly anisotropic; thus it is not surprising that the thermally activated collective motions of the globin are anisotropic as well. This observation of a large dynamic change in the phase anisotropy on ~1 ps time scales is consistent with a recent suggestion by Hochstrasser and co-workers that cooling of the heme may proceed in part via coupling to highly anisotropic collective motions of the globin.[36] Their estimate of 0.23−2.3 ps for the relevant time scales of energy flow from heme to solvent via collective modes was based on the estimated group velocities in the globin (1−10 nm/ps) and the global dimensions of the protein (~2−4 nm diameter).[45] The increase in the phase anisotropy from r_{Re}(500 fs) = 0.2 at low pump powers to r_{Re}(500 fs) = 0.4 at high powers points toward the increased role at higher temperatures of collective, highly directed protein motions in transferring thermal energy from the heme to the surrounding globin and solvent.

D. Directed Structural Relaxation in Proteins. The protein strain contributions displayed in Figure 8 show that the protein undergoes a clear change in its shape within less than 500 fs following photodissociation. Decomposing the residual grating signals into in-plane and out-of-plane components indicates that the protein lengthens along the normal to the heme plane. This observation is consistent with the known differences in the equilibrium X-ray structures of MbCO and deoxyMb.[46] Relative to MbCO, the atoms comprising the EF helices in deoxyMb are globally displaced away from the proximal side of the heme plane (the side of the heme plane opposite the CO binding site). This motion is driven by the out-of-plane motion of the iron and the ensuing repulsive interaction between the iron and the proximal histidine and adjacent contacts to the F helix. The mechanics of this motion can be likened to tipping the fulcrum (heme doming site) of a lever (the EF helical section). There are other motions involving other regions closely coupled to the heme (e.g., C, H helical regions), but it is this motion of the EF helical sections that constitutes the allosteric core in

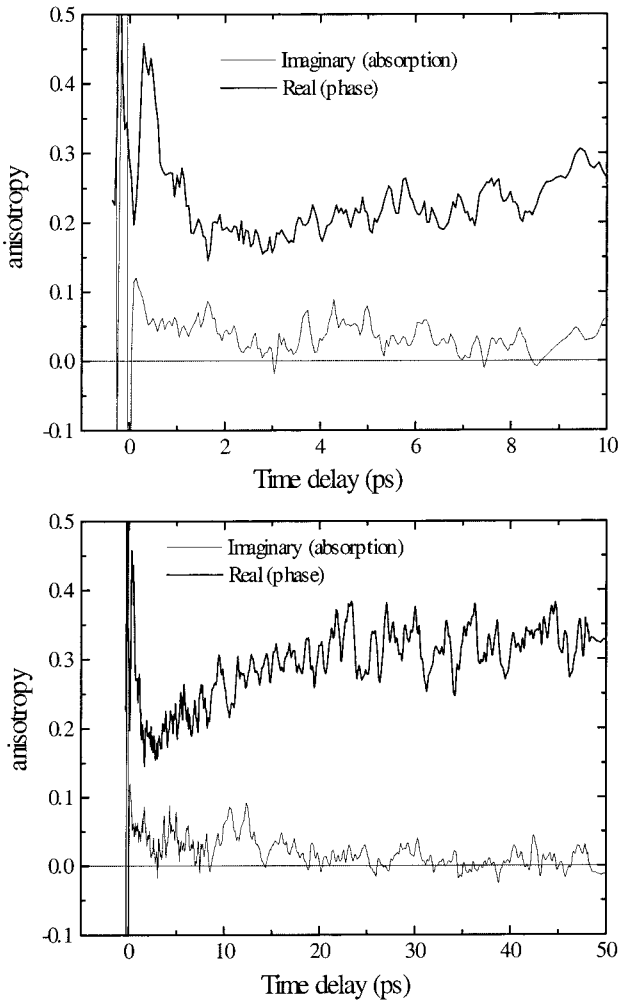

Figure 12. Phase and absorption anisotropies for MbCO at high excitation energy (U_{ex} = 12 μJ). The magnitudes of the high-power anisotropies are consistently lower than in the low-power case (Figures 3 and 6), following the expected saturation behavior.

directing the forces. In concert with this lateral motion of the EF helices, there is also a slight outward displacement along the normal to the heme plane. To help make the connection of the observable to microscopic processes, schematic representations of the most important motions have been given elsewhere.[11,14] These various displacements would lead to a change in shape in the protein. Motion of the EF helices parallel to the heme plane would increase the number of protein atoms per unit area projected along the heme plane and the slight outward motion would decrease the number of protein atoms per unit area along the heme normal. The corresponding change in the index of refraction requires information on the change in volume element and summing over contributions from both solvent and protein polarizability contributions. Irrespective, the net effect would be to change the shape of the protein in a manner consistent with experimental observations.

It should be born in mind that the differences in equilibrium structures between MbCO and deoxyMb do not involve CO within the heme pocket, whereas the photogenerated deoxyMb has the CO within the heme pocket/protein for several hundred nanoseconds. The ligand is not an insignificant perturbation. By extending the time base of the grating studies, we have recently determined that the CO diffusion out of the protein leads to a comparable change in protein strain as the initial bond breaking event.[47] The structural changes associated with ligand diffusion in and out of the protein are thought to involve primarily the distal side.[7] Time-resolved diffraction experiments with picosecond resolution will be required to determine the dominant motions responsible for the present experimental observations. The main point is that the potential energy surface of the protein is poised to drive atomic displacements that would lead to a change in shape of the protein.

The fast time scale of these motions points toward the involvement of collective mechanical modes of the globin in transducing the energy liberated by the initial bond break into specific displacements of atoms within the molecule. An analysis of the differences in structure between the deoxy and oxy tertiary structures of myoglobin illustrated that the two structures could be reproduced to within 60% accuracy by the displacement of the lowest frequency collective modes in the range of 5−12 cm^{-1}.[13] From studies of energy relaxation in heme proteins, it is clear that modes in this frequency range are very strongly damped.[10,12,35] The results from the studies of deoxyMb (and comparable relaxation components for MbCO) are in agreement with earlier work that has determined that large amounts of excess energy (>10 000 cm^{-1}) can be dissipated into the surrounding solvent on picosecond time scales. Under high excitation conditions, MbCO is found to exhibit a power-dependent feature with subpicosecond components that was attributed to increased anharmonic coupling between the collective modes of the protein and increased spatial dispersion of the larger amount of excess energy. Thus, proteins are strongly anharmonic systems in which energy dispersion and dissipation processes occur on time scales comparable to the periods of the lowest frequency collective modes, so that most of the driven motion occurs within a half period for these strongly damped modes. In this regard, the half-period motion of the 12 cm^{-1} mode is within a factor of 2 of the experimental observations. Given the approximate nature of the potentials used in the analysis,[13] this degree of agreement is relatively good. Similar arguments could be made on the basis of speeds of sound within the protein. Motions driven by a central force involving collective displacements over the protein radius (15 Å) could occur on subpicosecond time scales within a range of suitable sound velocities (10^5 and 5×10^5 cm/s), as observed. Thus, the observed time scale is understandable almost exclusively within a collective mode basis. More relevant may be the close connection between the observed dynamics for the development of the protein's anisotropic strain and the damping time for the coherently excited Raman active modes of the heme—in particular the heme doming mode.[17] The near coincidence in dynamics indicates that the heme doming coordinate is directly coupled to the collective modes of the protein. This provides a simple mechanical model for understanding how the reaction forces are so efficiently channeled into functionally relevant motions. On the time scale of the heme doming, the helical structures behave rigidly and as such are displaced as a unit by this force; i.e., the constituent atoms of the secondary structures move collectively.

The dynamics for the anisotropic protein strain, acoustic nature of the motions,[10,11] and close correspondence to the relaxation dynamics at the heme site[12,11] indicate the initial structural relaxation is largely derived from the coupling of the reaction forces to the collective modes of the protein. This relaxation phase results from the larger net displacement of the inertial modes of the protein along the reaction coordinate, in response to the reaction forces, than the spurious motions orthogonal to this coordinate. The relative importance of the inertial response to relaxation dynamics has now been well established for the liquid state.[48,49] So it might be expected that

inertial-like dynamics would also play a role in proteins. However, with a few possible exceptions,[50] there has been virtually no evidence for preferential or anisotropic coupling to liquid modes/relaxations. The homogeneous nature of the medium and orientational averaging effects of the solvent molecules most likely account for the absence of a pronounced effect in liquids. The distinction of this work is that it has been possible to observe mode-selective coupling in proteins that leads to anisotropic strain. It is the very nature of the protein's highly asymmetric heterogeneous structure to preferentially direct reactions. In the context of the allosteric regulation of heme proteins, nonuniform displacements are the key signature of a directed process. From the observed dynamics for the phase anisotropy, we conclude that the "director" for transducing reaction forces into functionally relevant motions are the collective modes of the protein. The long-range correlations mediated through the secondary structures of proteins would act to enhance the coupling of the reaction forces to the collective motions of the protein over comparable processes in the liquid state. The observation that the most significant mode-selective coupling or anisotropic strain ($t < 1$ ns) occurs through the inertial or nondiffusive relaxation phase illustrates how strongly guided reaction coordinates are in biological systems. Indeed, the highly concerted motions can be likened to a conformational switch, as suggested by recent high-resolution structure determinations of MbCO and deoxyMb[14] and modal analysis of the structural differences.[13]

IV. Conclusion

A detailed analysis and comparison of the information content of the heterodyne-detected transient grating signals from MbCO, PHCO, and deoxyMb has been undertaken. The dynamics of the electronic-state evolution can be inferred by examining the Im components of the grating signals in light of previous studies. The Re signals provide information on thermal and conformational relaxation in the protein. The primary new observation is that the phase anisotropy increases far past the value allowed by the change in the electronic state of the heme upon conversion from the CO-ligated to deligated forms. Comparison of the grating signals of MbCO and PHCO allows removal of the electronic contributions, revealing a large residual phase anisotropy that is attributed to asymmetric conformational relaxation in the protein. The <0.5 ps development of anisotropic protein strain implies that photodissociation of the heme−CO bond activates the collective motions of the protein to drive the system from its ligated to deligated conformational distribution.

Acknowledgment. This work was supported by the Natural Sciences and Engineering Research Council of Canada and Photonics Research Ontario.

References and Notes

(1) Goodno, G. D.; Miller, R. J. D. *J. Phys. Chem. A* **1999**, *103*, 10619 and references therein.
(2) Petrich, W. J.; Poyart, C.; Martin, J. L. *Biochemistry* **1988**, *27*, 4049.
(3) Murray, L. P.; Henry, E. R.; Eaton, W. A. *Biophys. Chem.* **1988**, *29*, 63.
(4) Frauenfelder, H.; Sligar, S. G.; Wolynes, P. G. *Science* **1991**, *254*, 1598.
(5) Anfinrud, P.; Hochstrasser, R. M. *Proc. Natl. Acad. Sci. U.S.A.* **1989**, *86*, 8387.
(6) Leeson, D. T.; Wiersma, D. A.; Fritsch, K.; Friedrich, J. *J. Phys. Chem.* **1997**, *101*, 6331.
(7) Tian, W. D.; Sage, J. T.; Champion, P. M.; Chien, E.; Sligar, S. G. *Biochemistry* **1996**, *35*, 3487.
(8) Ansari, A.; Jones, C. M.; Henry, E. R.; Hofrichter, J.; Eaton, W. *Science* **1992**, *256*, 1796.
(9) Jackson, T. A.; Lim, M.; Anfinrud, P. A. *Chem. Phys.* **1994**, *180*, 131.
(10) Genberg, L.; Richard, L.; McLendon, G.; Miller, R. J. D. *Science* **1991**, *251*, 1051; Genberg, L.; Heisel, F.; McLendon, G.; Miller, R. J. D. *J. Phys. Chem.* **1987**, *91*, 5521.
(11) Deak, J.; Chiu, H. L.; Lewis, C. M.; Miller, R. J. D. *J. Phys. Chem. B* **1998**, *102*, 6621.
(12) Miller, R. J. D. *Acc. Chem. Res.* **1994**, *27*, 145.
(13) Seno, Y.; Go, N. *J. Mol. Biol*. **1990**, *216*, 111.
(14) Kachalova, S. G.; Popov, A. P.; Bartunik, H. D. *Science* **1999**, *284*, 473.
(15) Gibson, Q. H.; Antonini, E. *J. Biol. Chem.* **1963**, *238*, 1384.
(16) Smith, M. H. *Biochem. J.* **1959**, *73*, 90.
(17) Tian, W. D.; Sage, J. T.; Srajer, V.; Champion, P. M. *Phys. Rev. Lett.* **1992**, *68*, 408.
(18) Goodno, G. D.; Miller, R. J. D. Patent pending.
(19) Herman, P. R.; Goodno, G. D.; Gu, X.; Kalbfleisch, J. B.; Long, J.; Lukacs, M.; Marjoribanks, R. S.; Miller, R. J. D.; Nantel, M.; Ness, S.; Oettl, T. In *Laser Applications in Microelectronic and Optoelectronic Manufacturing IV*; Dubowski, J. J., Helvajian, H., Kreutz, E. W., Sugioka, K., Eds.; SPIE Proceedings; SPIE: Bellingham, WA, 1999; No. 3616.
(20) Nelson, K. A.; Miller, R. J. D.; Lutz, D. R.; Fayer, M. D. *J. Appl. Phys.* **1982**, *53*, 1144.
(21) Hellwarth, R. W. *Prog. Quantum Electr*. **1977**, *5*, 1.
(22) Goodno, G. D.; Astinov, V.; Miller, R. J. D. *J. Phys. Chem. B* **1999**, *103*, 603.
(23) Lim, M.; Jackson, T. A.; Anfinrud, P. A. In *Ultrafast Phenomena VIII*; Martin, J.-L., Migus, A., Mourou, G. A., Zewail, A. H., Eds.; Springer-Verlag: Berlin, 1993; p 522.
(24) Lim, M.; Jackson, T. A.; Anfinrud, P. A. *J. Phys. Chem*. **1996**, *100*, 12043.
(25) McMorrow, D.; Lotshaw, W. T.; Kenney-Wallace, G. A. *IEEE J. Quantum Electron* **1988**, *24*, 443.
(26) Dickson, T. R. In Ph.D. Dissertation, Physics Department, University of Toronto, Toronto, Ont., 1991; p 151.
(27) Vohringer, P.; Scherer, N. F. *J. Phys. Chem*. **1995**, *99*, 2684.
(28) Eaton, W. A.; Hofrichter, J. *Methods Enzymol*. **1981**, *76*, 175.
(29) Makinen, M. W.; Churg, A. K. In *Iron Porphyrins, Part I*; Lever, A. B. P., Gray, H. B., Eds.; Addison-Wesley: Reading, MA, 1983; p 141.
(30) Schomaker, K. T.; Bangcharoenpaurpong, O.; Champion, P. M. *J. Chem. Phys.* **1984**, *80*, 4701.
(31) Jackson, T. A.; Lim, M.; Anfinrud, P. A. *Chem. Phys.* **1994**, *180*, 131.
(32) Istratov, A. A.; Vyvenko, O. F. *Rev. Sci. Instrum.* **1999**, *70*, 1233.
(33) Martin, J. L.; Migus, A.; Poyart, C.; Lecarpentier, Y.; Astier, R.; Antonetti, A. *Proc. Natl. Acad. Sci. U.S.A.* **1983**, *80*, 173.
(34) Miller, R. J. D. *Annu. Rev. Phys. Chem.* **1991**, *42*, 581.
(35) Mizutani, Y.; Kitagawa, T. *Science* **1997**, *278*, 443.
(36) Lian, T.; Locke, B.; Kholodenko, Y.; Hochstrasser, R. M. *J. Phys. Chem.* **1994**, *98*, 11648.
(37) Henry, E. R.; Eaton, W. A.; Hochstrasser, R. M. *Proc. Natl. Acad. Sci. U.S.A.* **1986**, *83*, 8982.
(38) Peterson, K. A.; Rella, C. W.; Engholm, J. R.; Schwettman, H. A. *J. Phys. Chem. B* **1999**, *103*, 557.
(39) Chernoff, D. A.; Hochstrasser, R. M.; Steele, A. W. *Proc. Natl. Acad. Sci. U.S.A.* **1980**, *77*, 5606.
(40) Montant, S.; Le Calvez, A.; Freysz, E.; Ducasse, A.; Couzi, M. *J. Opt. Soc. Am. B* **1998**, *15*, 2802.
(41) Palese, S.; Schilling, L.; Miller, R. J. D.; Staver, P. R.; Lotshaw, W. T. *J. Phys. Chem*. **1994**, *98*, 6308.
(42) Deak, J.; Pereira, M.; Richard, L.; Chiu, H. L.; Miller, R. J. D. *Methods Enzymol*. **1994**, *232*, 322.
(43) Richard, L.; Genberg, L.; Deak, J.; Chiu, H. L.; Miller, R. J. D. *Biochemistry* **1992**, *31*, 10703.
(44) Kenkre, V. M.; Tokmakoff, A.; Fayer, M. D. *J. Chem. Phys.* **1994**, *101*, 10618.
(45) Dickerson, R. E.; Geiss, I. *HemoglobIn Structure, Function, Evolution, and Pathology*; Benjamin Cummings: Menlo Park, CA, 1983.
(46) Kuriyan, J.; Wilz, S.; Karplus, M.; Petsko, G. A. *J. Mol. Biol.* **1986**, *192*, 133.
(47) Dadusc, G.; Goodno, G. D.; Chiu, H. L.; Ogilvie, J.; Miller, R. J. D. *Isr. J. Chem.* **1998**, *38*, 191.
(48) Jemenez, R.; Fleming, G. R.; Kumar, P. V.; Maroncelli, M. *Nature* **1994**, *369*, 471.
(49) Maroncelli, M. *J. Mol. Liq.* **1993**, *57*, 1.
(50) Wang, C.; Akhremitchev, B. B.; Walker, G. C. *J. Phys. Chem. A* **1997**, *101*, 2735.